[9]K. Zeppenfeld, Z. Physik, 211, 391 (1968).
[10]E. A. Taft and H. R. Phillip, Phys. Rev. 138, A197 (1965).
[11]G. Priftis, Phys. Rev. B 2, 54 (1970).
[12]T. Suzuki, T. Kishimoto, T. Kaji, and Ts. Suzuki, J. Phys. Soc. Japan 29, 730 (1970).
[13]O. Aita, I. Nagakura, and T. Sagawa, J. Phys. Soc. Japan 30, 516 (1970).
[14]T. Suzuki and A. Tanokura, J. Phys. Soc. Japan 30, 892 (1971).
[15]C. Koumelis, D. Leventouri, and K. Alexopoulos, Phys. Status Solidi (b) 46, K89 (1971).
[16]A. Nilson, Arkiv Physik 6, 516 (1953).
[17]A. Theodossiou and P. Vosnides, Phys. Rev. 145, 458 (1966).
[18]J. Crowell and R. H. Ritchie, Phys. Rev. 172, 436 (1968).

PHYSICAL REVIEW B VOLUME 7, NUMBER 1 1 JANUARY 1973

# Electron-Paramagnetic-Resonance Study of $3d^5$ Ions in Mixed-Polytype Zinc Sulfide

T. Buch, B. Clerjaud, and B. Lambert
*Laboratoire de Luminescence* II, *Equipe de Recherches associée au Centre National de la Recherche Scientifique, Université de Paris* VI - 75 *Paris* 5*e*, *France*

and

P. Kovacs
*Research Institute for Technical Physics of the Hungarian Academy of Sciences, Budapest, Ujpest* 1, *Pf.* 76, *Hungary*
(Received 8 May 1972)

Mixed-polytype ZnS single crystals doped with various $3d^5$ ions ($Cr^+$, $Mn^{++}$, and $Fe^{3+}$) have been examined by electron-paramagnetic-resonance techniques. It was found that three kinds of sites exist in these crystals, one of cubic and two of axial symmetry around the *c* axis of these "hexagonal" crystals. None of the axial centers correspond to the one characteristic of a true wurtzite crystal. A model of the crystallographic nature of these centers based on a point-charge calculation is proposed which allows a qualitative understanding of the experimental facts.

## I. INTRODUCTION

Optical measurements on "hexagonal" ZnS crystals doped with various $3d^n$ ions ($Cu^{2+}$,[1,2] $Cr^{2+}$,[3] and $Fe^{2+}$ [4]) have demonstrated the existence of centers of axial symmetry in these crystals in addition to the known "cubic" centers. In reality, these so-called "hexagonal" crystals are of mixed-polytype structure, and one can have several different axial sites, at least in principle. Furthermore, the splittings of levels due to the low-symmetry fields add to the complexity of the optical spectra.

The observation of electron-paramagnetic-resonance (EPR) signals of $3d^5$ ions whose ground state is an orbital singlet ($Cr^+$, $Mn^{2+}$, and $Fe^{3+}$) eliminates the complexity due to orbital splitting and gives clear evidence of the axial-symmetry centers. We have thus detected *two* kinds of axial sites in these crystals (in addition to cubic) for each of the isoelectronic doping ions. These two sites, whose spin-Hamiltonian parameters we measured, are occupied with about equal numbers of doping ions.

The axial field parameters vary greatly from one ion to another, and for some ions, from one site to the other. For $Fe^{3+}$, moreover, second-order terms in the spin-Hamiltonian formalism are important; this necessitates special care in the evaluation of the spectra, and a formalism to this end has been developed.

A point-charge crystal-field calculation on various polytype structures permits one to explain the presence of these centers, as well as the fact that not more than two different axial sites appear in these crystals; none of which corresponds to the site characteristic of a true hexagonal (wurtzite) structure.

The three $3d^5$ centers play important roles in the luminescence mechanisms in ZnS. $Mn^{2+}$ is well known for its yellow-orange emission; $Cr^+$ is a filled electron trap. $Fe^{3+}$ is a recombination center in the middle of the forbidden gap.

The specific influence of the axial sites on the luminescence of these crystals is at present being studied in this laboratory.

## II. EXPERIMENTAL

All samples used were synthetic and growth doped. They are all of those commercially called "hexagonal", although their contents in "hexagonalicity" is widely variable. We have examined bulk single crystals of three different origins: (i) vapor-phase-grown crystals of the Research Insti-

tute for Technical Physics of the Hungarian Academy of Sciences. These crystals contain mainly Fe;[5] concentration used varied from $10^{-3}$–$10^{-4}$ atom-g Fe per mol ZnS; (ii) crystals obtained by fusion of ZnS powder under high pressure, made at the Institute of Solid State Physics of the University of Tokyo. These samples ($J$-193) contain $10^{-6}$ atom-g Cr per mol ZnS; (iii) melt-grown crystals, from Eagle-Pitcher Industries, Inc., Miami, Okla. The samples $Z$-410 and $Z$-474 contain $10^{-4}$ atom-g Mn per mol ZnS. The sample $Z$-904 contains $10^{-4}$ atom-g Cr per mol ZnS.

EPR measurements on these samples have been made on an $X$-band spectrometer Varian Model No. V 4502 with a microwave bridge made in the laboratory,[6] and on a Varian Model No. V 4503 $K_a$-band spectrometer. Temperatures were varied by a nitrogen-circulation system Varian Model No. 4557.

### III. SPIN HAMILTONIAN AND POSITION OF LINES

The spin Hamiltonian for a $3d^5$ ion in a site of $C_{3v}$ symmetry can be written

$$\mathcal{H}_s = g\mu_B \vec{H}\cdot\vec{S} + A\vec{I}\cdot\vec{S} + \tfrac{2}{3}DO_0^{(2)} - \tfrac{2}{45}(a-F)O_0^{(4)} + \tfrac{2}{45}\sqrt{\tfrac{10}{7}}\,a(O_3^{(4)} - O_{-3}^{(4)}) \ . \quad (1)$$

In writing this expression we neglect explicitly the very small anisotropy of $g$ and $A$. $a$ is the cubic crystal-field parameter and $D$ and $F$ are the axial field parameters of the 2nd and 4th degree. The equivalent spin operators $O_q^{(k)}$ are given[7] in irreducible tensor form, and they correspond to Racah's $C_q^{(k)}$. We have chosen the crystal $c$ axis ([111] in cubic notation) as the axis of quantization, with the $x$ and $y$ axis being, in cubic notation, $[11\bar{2}]$ and $[\bar{1}10]$. We have neglected higher-order terms, as well as superhyperfine interactions and nuclear Zeeman and quadrupole terms.

Since in the usual EPR experiments the Zeeman interaction is dominant over all the other terms in $\mathcal{H}_s$, it is convenient to quantize along the external magnetic field $\vec{H}$, whose direction is given by the polar angles $\theta$ defined relative to the crystal $c$ axis [00.1] and $\psi$ the rotation angle of the crystal around the $c$ axis measured from the (11.0) plane. For the expression of the transformation of the $O_q^{(k)}$ to the new axis system, we can, without loss of generality, take the third Eulerian angle $\alpha$ to be zero. We have then

$$O_q^{(k)}(\omega) = \textstyle\sum_{q'} O_{q'}^{(k)}(\Omega) D^k_{q',q}(0,\theta,\psi) \ . \ .$$

Here, $\Omega$ symbolizes the polar coordinates relative to $\vec{H}$, $\omega$ symbolizes those relative to $c$, and $D^k_{q',q}(\alpha,\theta,\psi)$ are the Wigner-rotation matrix elements for $l=k$. In the new reference frame, $\mathcal{H}_s$ takes the form

$$\mathcal{H}_s = g\mu_B \vec{H}\cdot\vec{S} + A\vec{I}\cdot\vec{S} + \frac{2}{3}\left(\frac{2}{5}\right)^{1/2} D \sum_{m=-2}^{2}\left(-\frac{m}{|m|}\right)^m O_m^{(2)}\Theta_2^{|m|} - \frac{2\sqrt{2}}{135}(a-F)\sum_{m=-4}^{4}\left(-\frac{m}{|m|}\right)^m O_m^{(4)}\Theta_4^{|m|} + \frac{a}{180}\sum_{m=-4}^{4} V_m O_m^{(4)} \ , \quad (2)$$

where $\Theta_l^{|m|} = \Theta_l^{|m|}(\theta)$ are normalized Legendre functions,[8] and the $V_m$ are given by

$$V_0 = 20\sqrt{2}\,\sin^3\theta\cos\theta\cos 3\psi \ ,$$

$$V_{\pm1} = \pm\sqrt{\tfrac{5}{2}}\sin^2\theta\{[\,3(1-\cos\theta)^2 - 5\sin^2\theta\,]e^{\pm3i\psi} + [\,3(1+\cos\theta)^2 - 5\sin^2\theta\,]e^{\mp3i\psi}\} \ ,$$

$$V_{\pm2} = -\sqrt{5}\,\sin\theta\{(1-\cos\theta)[\,(1-\cos\theta)^2 - 3\sin^2\theta\,]e^{\pm3i\psi} - (1+\cos\theta)[\,(1+\cos\theta)^2 - 3\sin^2\theta\,]e^{\mp3i\psi}\} \ ,$$

$$V_{\pm3} = \pm\sqrt{\tfrac{5}{14}}\{(1-\cos\theta)^2[\,(1-\cos\theta)^2 - 7\sin^2\theta\,]e^{\pm3i\psi} + (1+\cos\theta)^2[\,(1+\cos\theta)^2 - 7\sin^2\theta\,]e^{\mp3i\psi}\} \ ,$$

$$V_{\pm4} = 2\sqrt{\tfrac{5}{7}}\,\sin\theta\,[(1-\cos\theta)^3 e^{\pm3i\psi} - (1+\cos\theta)^3 e^{\mp3i\psi}] \ .$$

With this spin Hamiltonian, a second-order perturbation calculation within the ${}^6A_1$ ground state of a $3d^5$ ion without nuclear spin gives the following positions of the $\Delta M_s = +1$ transitions: for $\vec{H}\parallel\vec{c}$,

$$H_{\parallel}(\pm\tfrac{5}{2}\leftrightarrow\pm\tfrac{3}{2}) = H_0 \mp 4D' \pm \tfrac{4}{3}(a'-F') - \tfrac{20}{27}(a'^2/H_0) \ ,$$

$$H_{\parallel}(\pm\tfrac{3}{2}\leftrightarrow\pm\tfrac{1}{2}) = H_0 \mp 2D' \mp \tfrac{5}{3}(a'-F') + \tfrac{20}{27}(a'^2/H_0) \ ,$$

$$H_{\parallel}(\tfrac{1}{2}\nrightarrow -\tfrac{1}{2}) = H_0 - \tfrac{40}{27}(a'^2/H_0) \ ; \quad (3)$$

and for $\vec{H}\perp\vec{c}$,

$$H_{\perp}(\pm\tfrac{5}{2}\leftrightarrow\pm\tfrac{3}{2}) = H_0 \pm 2D' \pm \tfrac{1}{2}(a'-F') + (1/H_0)[D'^2 - \tfrac{5}{4}D'(a'-F') - \tfrac{5}{144}(a'-F')^2 - \tfrac{5}{18}a'^2] \ ,$$

$$H_{\perp}(\pm\tfrac{3}{2}\leftrightarrow\pm\tfrac{1}{2}) = H_0 \pm D' \mp \tfrac{5}{8}(a'-F') - (1/H_0)[\tfrac{5}{4}D'^2 + \tfrac{5}{8}D'(a'-F') + \tfrac{425}{2304}(a'-F')^2 + \tfrac{25}{36}a'^2] \ ,$$

$$H_{\perp}(\tfrac{1}{2}\nrightarrow -\tfrac{1}{2}) = H_0 + (1/H_0)[-2D'^2 + \tfrac{5}{2}D'(a'-F') + \tfrac{5}{72}(a'-F')^2 + \tfrac{5}{9}a'^2] \ . \quad (4)$$

In these expressions, we have $H_0 = h\nu/g\mu_B$; $D' = D/g\mu_B$; $a' = a/g\mu_B$; and $F' = F/g\mu_B$. In a wurtzite-type single crystal, there are two magnetically nonequivalent sites related to each other by a rotation of $\frac{1}{3}\pi$ around the $c$ axis. These two types of sites exist also for the axial centers in the polytypes. This leads generally to a splitting of the

lines. For the central $\frac{1}{2} \rightarrow -\frac{1}{2}$ line this splitting is, to second order,

$$\delta H_{1/2 \rightarrow -1/2} = \tfrac{10}{3}\sqrt{2}\,\big|\,(a'/H_0)\sin^3\theta\cos\theta\cos 3\psi \times[2D'(11\cos^2\theta - 2) + \tfrac{1}{9}(a' - F')(175\cos^4\theta - 150\cos^2\theta + 33)]\,\big|\,. \quad (5)$$

This allows the measurement of $a$.

## IV. EXPERIMENTAL RESULTS

### A. $Fe^{3+}$

At liquid-nitrogen temperature and under uv illumination, besides the well-known spectrum of $Fe^{3+}$ in a site of cubic symmetry,[9,10] these crystals display supplementary lines which we interpret as being due to two centers with axial symmetry. For $\vec{H}$ parallel to the $c$ axis, we observe a set of four well-separated lines which we attribute to the transitions $\pm\frac{3}{2} \longleftrightarrow \pm\frac{1}{2}$, and two broad lines corresponding each to the superposition of two $\pm\frac{5}{2} \longleftrightarrow \pm\frac{3}{2}$ lines. The axial $\frac{1}{2} \rightarrow -\frac{1}{2}$ lines are indistinguishable from the cubic $\frac{1}{2} \rightarrow -\frac{1}{2}$ line. For $\vec{H}$ perpendicular to the $c$ axis, we see only one $\frac{1}{2} \rightarrow -\frac{1}{2}$ distinct line of the cubic transition, two $\pm\frac{3}{2} \longleftrightarrow \pm\frac{1}{2}$ and two $\pm\frac{5}{2} \longleftrightarrow \pm\frac{3}{2}$ lines.

At other orientations, all lines other than $\frac{1}{2} \rightarrow -\frac{1}{2}$ broaden and are no longer observed. This effect has also been observed for the cubic spectrum.[11] The $\frac{1}{2} \rightarrow -\frac{1}{2}$ lines corresponding to the two axial centers are unresolved, but they are split because of the two nonequivalent sites related to each other by a rotation of $\frac{1}{3}\pi$ around the $c$ axis.

From the spectrum at $\vec{H}$ parallel to the $c$ axis [Eq. (3)], together with the analysis of the splitting of the $\frac{1}{2} \rightarrow -\frac{1}{2}$ line [Eq. (5)] at various orientations shown on Fig. 1, we obtain the parameters $g_{\parallel}$, $D$, $a$, and $a-F$, of the spin Hamiltonian of the two axial centers shown on Table I.

The signs of $D$ and $a-F$ are opposite to each other. Liquid-helium-temperature measurements do not permit one to determine the absolute signs of these parameters; at this temperature the sensitivity is too low and the fine-structure lines in our crystals are too broad for accurate measurements to be possible.

But if we make the two assumptions, that $|F| < |a|$ and $a > 0$ as in the cubic structure, it follows that $D$ must be negative.

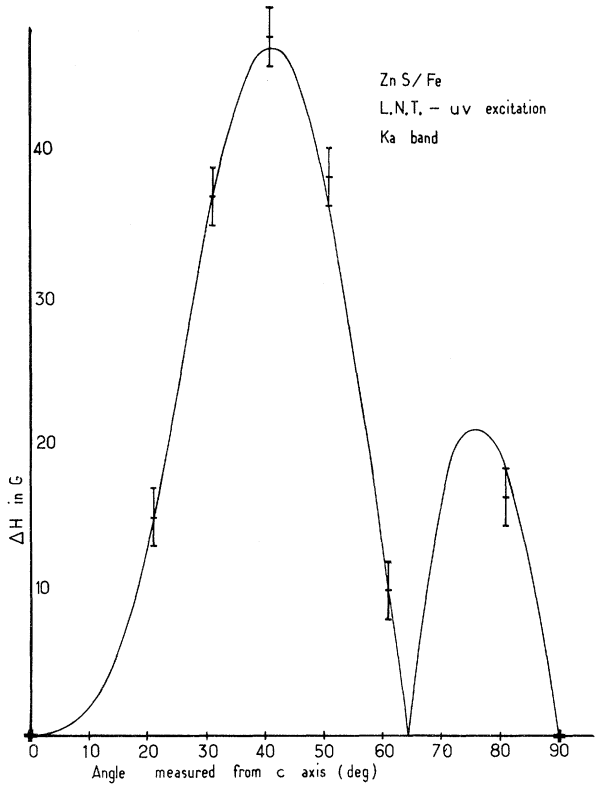


FIG. 1. Comparison of the angular variation of the splitting of the (unresolved) $\frac{1}{2} \rightarrow -\frac{1}{2}$ lines of the two axial centers, at $Ka$ band and $\psi = 0$, with theoretical values calculated by expression (5). Experimental values and their errors are represented by vertical bars. The full line corresponds to $D = -470\times10^{-4}$ cm$^{-1}$, $a-F = 159.7\times10^{-4}$ cm$^{-1}$, $a = 127\times10^{-4}$ cm$^{-1}$, and $H_0 = 12.494$ G. These parameters correspond to the average of those given in Table I. L. N. T. stands for liquid-nitrogen temperature.

For $\vec{H}$ parallel to the $c$ axis, the influence of higher-order terms is less than 0.2% at $X$-band frequencies. For $\vec{H}$ perpendicular to the $c$ axis, these terms may be important (10%) at $X$-band frequencies, but less than 1% at the $Ka$ band. These values of the parameters explain well the fact that the $\pm\frac{3}{2} \longleftrightarrow \pm\frac{1}{2}$ lines are confounded for $\vec{H}$ perpendicular to the $c$ axis.

Our values have been further confirmed by the

TABLE I. Spin-Hamiltonian parameters of $Fe^{3+}$ in mixed-polytype ZnS, at liquid-nitrogen temperature.

| | $\text{Axial}_1$ | $\text{Axial}_2$ | Cubic |
|---|---|---|---|
| $g_{\parallel}$ | $2.0194 \pm 0.0005$ | $2.0194 \pm 0.0005$ | $2.0194 \pm 0.0003$[a] |
| $a$ | $(127 \pm 5)\times10^{-4}$ cm$^{-1}$ | $(127 \pm 5)\times10^{-4}$ cm$^{-1}$ | $(127.4 \pm 0.5)\times10^{-4}$ cm$^{-1}$ [b] |
| $D$ | $(-479.9 \pm 5)\times10^{-4}$ cm$^{-1}$ | $(-460.1 \pm 5)\times10^{-4}$ cm$^{-1}$ | ... |
| $a$-$F$ | $(132.7 \pm 2)\times10^{-4}$ cm$^{-1}$ | $(186.7 \pm 2)\times10^{-4}$ cm$^{-1}$ | ... |
| $F$ | $(-6 \pm 7)\times10^{-4}$ cm$^{-1}$ | $(-59.7 \pm 7)\times10^{-4}$ cm$^{-1}$ | ... |

[a]Reference 9.

[b]Reference 10.

good agreement between calculated and measured values of the angular variation of the $\frac{1}{2} \rightarrow -\frac{1}{2}$ line. To second order, the distance between the cubic central line and the unresolved two axial ones is (neglecting terms in $F'^2$)

$$(D'/H_0)\sin^2\theta\,[2D'(9\cos^2\theta - 1) + \tfrac{5}{6}(a' - F')(77\cos^4\theta - 48\cos^2\theta + 3)]\,, \quad (6)$$

on account of the fact that all centers have the same $a$. Comparison between theory and experiment is shown on Fig. 2.

The change of the parameters of the spin Hamiltonian with temperature between liquid-nitrogen temperature and 170 K is very weak. Above this temperature, the spectrum is no longer observed. The variation is so weak that it may be interpreted as being due to thermal expansion of the crystal,[12] as well as being due to a weak coupling of the center with the lattice. It does not seem that in the other hexagonal II-VI compounds ZnO [13] and CdS for instance, the axial field parameter $D$ for $Fe^{3+}$ is appreciably temperature dependant.

### B. $Mn^{2+}$

In addition to the cubic center[10,14] and to the axial center[14] previously reported, we have studied some lines which had been observed before[14] but not interpreted. We have interpreted them[15] as being due to a second axial center with the following parameters:

$$\left.\begin{aligned} D &= (36.1 \pm 0.5)\times 10^{-4}\ \text{cm}^{-1} \\ a - F &= (7.4 \pm 0.5)\times 10^{-4}\ \text{cm}^{-1} \end{aligned}\right\} \text{ at 300 K;}$$

the parameters of the "known" axial center being

$$\left.\begin{aligned} D &= -130.9\times 10^{-4}\ \text{cm}^{-1} \\ a - F &= 7.7\times 10^{-4}\ \text{cm}^{-1} \end{aligned}\right\} \text{ at 300 K,}$$

with the $g$, $A$, and $a$ parameters being the same for the two centers. The signs of $D$ and $a - F$ have been determined from liquid-helium-temperature measurements.

For these two centers, the variation of $D$ with temperature is very weak, their values being

$$D = (35.2 \pm 0.5)\times 10^{-4}\ \text{cm}^{-1}$$

and

$$D = -130.7\times 10^{-4}\ \text{cm}^{-1}$$

at liquid-nitrogen temperature.

In other hexagonal II-VI compounds, ZnO for example, it does not appear that the axial field parameter of $Mn^{++}$ is appreciably temperature dependant.

### C. $Cr^{+}$

In addition to the usual cubic center,[10,16] we have observed under uv irradiation two axial centers characterized by the following spin-Hamiltonian parameters at liquid-nitrogen temperature[17]:

$$D = (-28.7 \pm 0.2)\times 10^{-4}\ \text{cm}^{-1},$$

$$a - F = (3.7 \pm 0.2)\times 10^{-4}\ \text{cm}^{-1},$$

for the first one;

$$D = (38.7 \pm 0.2)\times 10^{-4}\ \text{cm}^{-1},$$

$$a - F = (3.7 \pm 0.2)\times 10^{-4}\ \text{cm}^{-1},$$

for the second one. The $g$ and $a$ parameters are, for the two centers, the same as for the cubic center. The signs of $D$ and $a$-$F$ have been determined from liquid-helium-temperature measurements. We observed that the $D$ parameters change strongly with temperature. For the two centers, the variation of $D$ with temperature represented on Fig. 3 is described by[18,19]

$$D(T) = D_0 + \delta \coth \hbar\omega/2kT\,, \quad (7)$$

with

$$D_0 = (7.9 \pm 4)\times 10^{-4}\ \text{cm}^{-1},$$

$$\delta = (-35.0 \pm 2)\times 10^{-4}\ \text{cm}^{-1},$$

$$\hbar\omega = 245 \pm 7\ \text{cm}^{-1},$$

for the first center, and with

$$D_0 = (14.9 \pm 5)\times 10^{-4}\ \text{cm}^{-1},$$

$$\delta = (23.3 \pm 3)\times 10^{-4}\ \text{cm}^{-1},$$

$$\hbar\omega = 340 \pm 10\ \text{cm}^{-1},$$

for the second one. This law of variation is due

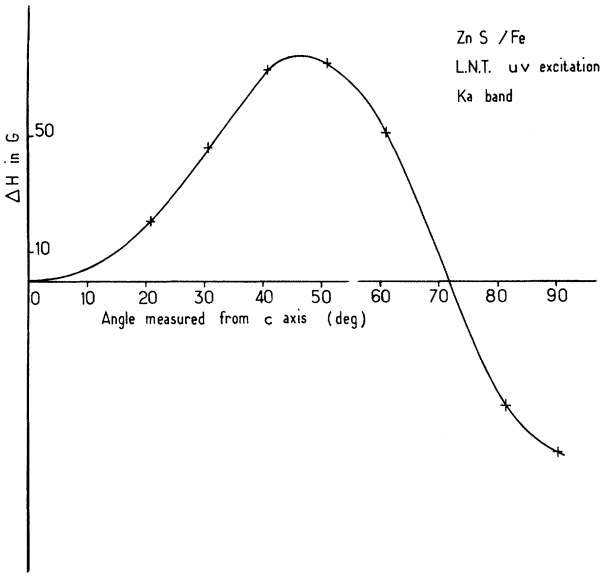


FIG. 2. Angular variation of the distance between the cubic and axial central lines at $Ka$ band. Comparison of experimental values (crosses) with Eq. (6). Same parameters as in Fig. 1.

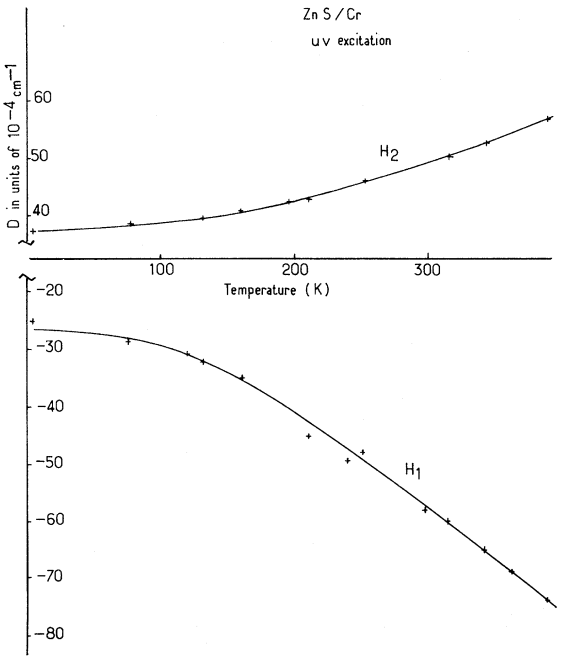


FIG. 3. Temperature dependence of the axial field parameter $D$. Experimental values are represented by crosses. Continuous lines correspond to the values calculated by means of the expression (7), with the values of parameters given in the text.

to the coupling of the center with the lattice, $\omega/2\pi$ being an effective phonon frequency.[19]

## V. DISCUSSION

For each of the three $3d^5$ ions studied, $Cr^+$, $Mn^{++}$, and $Fe^{+++}$, there appears to exist three different paramagnetic centers in "hexagonal" ZnS. One of these three centers displays cubic symmetry, the other two are "axial" centers. The existence of these sites is thus shown to be a property of these "hexagonal" ZnS crystals, independent of the ion which happens to occupy such a site, and should be interpreted on the basis of the structure of the crystals, as we discuss below.

On the other hand, the comparison between the properties of the three $3d^5$ substituent ions in these sites shows an extraordinary disparity between them. We might show the qualitative aspects of this comparison in Table II.

Let us discuss first the crystallographic nature of the three centers present. As is well known, the cubic and hexagonal forms of ZnS originate in differences in the stacking of successive anion and cation planes along the hexagonal [00.1] $c$ axis (which coincides with a cubic [111] direction for zinc blende). Viewed along this axis, each structure consists of alternate Zn- and S-atom layers; such a double layer can be thought of as composed of pairs of a Zn and a S atom, with all the "molecular" axes oriented along $c$.

We have thus a sequence of ZnS layers or double planes, which we symbolize $A\alpha$, $B\beta$, or $C\gamma$. These three kinds of layers are equivalent but differ by a shift of their origin by $\frac{1}{3}n\vec{u}$, $\vec{u}$ being a vector defined in Fig. 4(a). For $n=1$ or 2, one arrives at the configurations of Fig. 4(b) or 4(c).

All crystalline forms of ZnS, both "pure" and polytypes, are expressed in terms of sequences of these layers. Thus wurtzite is $A\alpha B\beta A\alpha B\beta$, zinc blende is $A\alpha B\beta C\gamma A\alpha B\beta C\gamma$; and the polytype $6H$, which we take as an example, is $A\alpha B\beta C\gamma A\alpha C\beta B\gamma$. We write in each case the structure of each layer as $M\mu$ to emphasize the lack of reflection symmetry perpendicularly to the $c$ axis. To represent different stacking sequences we use the method illustrated in Fig. 5. In this figure, an $A$ plane is represented as a full line without an arrow, a $B$ plane as $\rightarrow$ and a $C$ plane as $\leftarrow$; the corresponding $\alpha$, $\beta$, or $\gamma$ are symbolized by broken lines. Distances along the $c$ axis are roughly rendered in the figure, as well as the configuration of successive neighboring planes. Thus we see that in each case the first neighbors of any one atom form a regular tetrahedron (which might be slightly deformed; but $c/a$ and $u$ values in ZnS are quite close to the ideal close-packing values of $\sqrt{\frac{8}{3}}$ and $\frac{3}{8}$, respectively); the second neighbors form a trigonal prism when the corresponding layers are equal, an antiprism otherwise. If the third next plane (which is formed of ions of opposite charges to those of the "central" one) has a configuration equal to that of the "central" one, there is a single third neighbor along the $c$ axis. But note that since the distances between the planes are not equal, this can take place only to one side, as one moves along $c$. In all other cases, this single third neighbor is absent.

Up to third neighbors we have the following four possible sites, which each depends upon a given sequence of four crystallographic layers; if $x$ is the layer which corresponds to the site considered, the prismatic configuration is obtained whenever

TABLE II. Qualitative aspects of the comparison between the two axial sites of the three ions $Cr^+$, $Mn^{2+}$, and $Fe^{3+}$. $D_0$ and $\delta$ are defined in Eq. (7).

| | $Fe^{+++}$ | $Mn^{++}$ | $Cr^+$ |
|---|---|---|---|
| $D_0$ | similar | very different; opposite signs | similar |
| $\delta$ | negligible | very small | large; different opposite signs |
| $F$ | very different | | |
| $a$-$F$ | different | equal | similar |

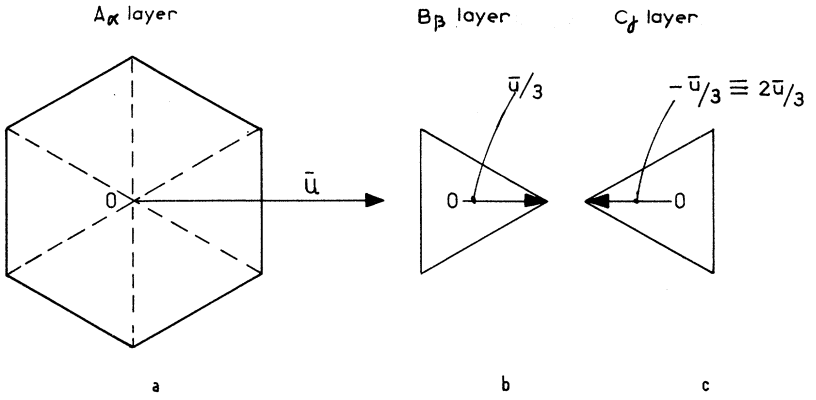


FIG. 4. Representation of the three kinds of layers: $a$ corresponds to $A\alpha$ layer, $b$ to $B\beta$ layer, and $c$ to $C\gamma$ layer. $A$, $B$, $C$ represents the Zn planes, $\alpha$, $\beta$, $\gamma$ represents the $S$ planes.

$x-1=x+1$; the single third neighbor exists whenever $x+2=x$. Thus, four sites may exist as follows:

$x-1=x+1$ ; $x+2\neq x$ PN ;

$x-1\neq x+1$ ; $x+2\neq x$ AN (zinc blende) ;

$x-1\neq x+1$ ; $x+2=x$ AS ;

$x-1=x+1$ ; $x+2=x$ PS (wurtzite) ,

where P indicates prismatic, A antiprismatic, S indicates the presence of a single-axial third neighbor, and N its absence. The last site, PS is characteristic of the wurtzite structure. This structure does not appear to exist in significant concentration in mixed polytypic bulk ZnS.[20] It can appear only in needle or platelets; thus we have just three sites present in all real crystals of ZnS. One can furthermore convince oneself that the sites PN and AS always occur side by side and thus in equal concentrations.

The relative proportion of prismatic sites in a mixed polytype is described by the "hexagonalicity" parameter $\alpha$. This parameter is given by

$$\alpha=[n_P]/([n_A]+[n_P]) , \tag{8}$$

where $[n_P]$ is the number of prismatic sites, $[n_P]=[n_{PN}]+[n_{PS}]$, and $[n_A]$ is the number of antiprismatic sites $[n_A]=[n_{AN}]+[n_{AS}]$. The birefringence of a given crystal has been shown[21,22] to be proportional to $\alpha$. We have therefore performed birefringence measurements on our crystals, in order to correlate $\alpha$ with the relative intensity of the axial EPR spectra. It is difficult to assure a good precision for these measurements since the EPR linewidths and shapes are quite different for the different sites. We find however that the intensities of both axial spectra are about equal, and the correlation of these intensities relative to the cubic "signal" with the birefringence is satisfactory. Table III gives the results for three crystals of different characteristics.

The crystalline field parameters should be quite different for the four sites. We have undertaken a calculation of some of these parameters in the point-charge approximation. We have, for the

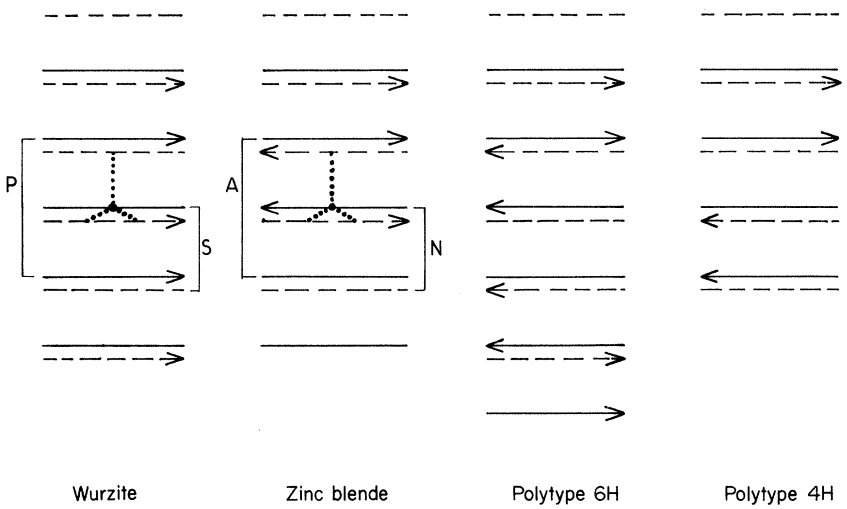


FIG. 5. Illustration of the method used to describe the layers defined in Fig. 4. An $A$ plane is represented as a full line without arrow, a $B$ plane as → and a $C$ plane as ←; the corresponding $\alpha,\beta,\gamma$ are symbolized by broken lines. In the case of wurtzite, the first neighbors form a tetrahedron, the second form a prism, and the third is single (*PS* site). In the case of zinc blende, the first neighbors form a tetrahedron the second form an antiprism, and there is no single third (*AN* site).

TABLE III. Correlation between the percentage of axial center ($H_1$ or $H_2$) and the hexagonalicity $\alpha$ defined in Eq. (8). The references of the single crystals are given in Sec. II.

| Crystal Ref. | Ion | $Axial_1$ (%) | $Axial_2$ (%) | Cub. (%) | $\alpha$ (%) |
|---|---|---|---|---|---|
| *Z* 904 | $Cr^+$ | 16±5 | 14±5 | 70±10 | 12.5±2 |
| *J* 191 | $Cr^+$ | 17±5 | 12±5 | 71±10 | 12±2 |
| *Z* 474 | $Mn^{++}$ | 7±3 | 8.5±3 | 84.5±6 | 7.7±1.3 |

potential, in terms of the Tesseral harmonics $C_{lm}$

$$V_c = \sum_{lm} \gamma_{lm} r^l C_{lm}(\theta, \varphi) , \tag{9}$$

where

$$\gamma_{lm} = \frac{4\pi}{2l+1} \sum_i \frac{q_i}{R_i^{l+1}} C_{lm}(\Theta_i, \Phi_i) ,$$

where $i$ designates the different ions whose charge is $q_i$ and polar coordinates $R_i, \Theta_i, \Phi_i$. The terms describing the axial field are

$$\gamma_2 \equiv \gamma_{20}, \quad \gamma_3 \equiv \gamma_{30} - \tfrac{1}{2}\sqrt{5}\ \gamma_{33}, \quad \gamma_4 = \gamma_{40} - \tfrac{1}{2}\sqrt{\tfrac{7}{5}}\ \gamma_{43} , \tag{10}$$

when $\theta$ is measured from the trigonal axis. These calculations were performed by means of a lattice sum over a large number of hexagonal unit cells, for several different crystal structures (zinc blende, wurtzite,[23] and several polytypes). It is found that the parameters calculated for the four sites PN, AN, AS, and PS are characteristic of each of these sites, and independent of the stacking sequence beyond the third neighboring planes. Thus the axial field at a given site is the same whatever the polytype. There will thus never be more than four centers. Table IV gives the values calculated for $\gamma_2$, $\gamma_3$, and $\gamma_4$ for these four centers.

The axial field of second order ($\gamma_2$) depends exclusively on the *N*-*S* character: the absence or presence of the single axial third neighbor. This does not mean that it is a single atom which contributes to $\gamma_2$. In fact $\gamma_2$ converges more slowly than $\gamma_4$ when one extends the "crystal" in a direction perpendicular to the *c* axis. Therefore the calculated values are not exactly zero for *N* sites.

The axial fields of third and fourth order $\gamma_3$ and $\gamma_4$ depend additively on both P and S characters. However, it should be remarked that they depend on a balance between terms, and are quite sensitive to distortions from the ideal packing of perfect tetrahedra.[24]

If we now consider the origin of the zero-field-splitting parameter *D*, it is well known that a large number of mechanisms contribute to its value.[25,26]

TABLE IV. Axial field parameter $\gamma_2$, $\gamma_3$, and $\gamma_4$ (atomic units $\times R^{l+1}$) defined in expression (10).

| | $\gamma_2$ | $\gamma_3$ | $\gamma_4$ |
|---|---|---|---|
| *AS* | −0.0563 | +0.077 | −0.0534 |
| *PS* | −0.0553 | −0.038 | +0.0367 |
| *AN* | −0.0043 | 0.0 | 0.0 |
| *PN* | −0.0041 | −0.117 | +0.0891 |

It is therefore difficult to make an estimate, without performing rather extensive calculations especially when covalency and overlaps are likely to be important as will be the case for $Fe^{3+}$. However, we may examine some general trends which tend to make the disparity of behavior between $Cr^+$ and $Mn^{++}$ qualitatively comprehensible.

In fact the different contributions of the "ion-multipole" model of Sharma *et al.*[25] all depend on the crystal-field parameters which measure the intensity of the axial fields of order 2 and 4, which both contribute to *D* in trigonal symmetry.[26] The odd fields may also contribute by the bias of an effective even field.[25] For a given site, the "ionic" part of *D* will be a balance of contributions of $\gamma_2\langle r^2\rangle$, $\gamma_4\langle r^4\rangle$ and $\gamma_3\langle r^3\rangle_{pd}$. If the crystal-field strength is assumed to be independent of the ion occupying the site, the different values of $\langle r^n\rangle$ for the various ions will produce different weights for these terms; this effect tends to make the contribution of $\gamma_4$ relatively more important for $Cr^+$ than for $Mn^{++}$. But as the ionic radius of $Cr^+$ is considerably larger than that of $Zn^{++}$, the field produced by local distortions of the lattice may be important but difficult to estimate. Both these effects contribute, however, to the temperature sensitivity of *D* for $Cr^+$.

Iron is dominated by covalency effects,[27,28] and these "ionic" contributions are largely insufficient to explain the large values of *D* for this ion. We may estimate that here, as it is the case for the other magnetic properties of this ion[29] charge transfer and the interaction of close-lying non-bonding $^6T_1$ levels dominate over the "ionic" crystal-field effects, thus accounting for the smallness of the difference between both axial centers.

## ACKNOWLEDGMENTS

We wish to thank Professor I. T. Steinberger for an extremely interesting discussion about the nature of ZnS polytypes and C. Barthou for the use of his computer programs for the crystal-field-parameter calculation. Mrs. Devaux-Morin performed the birefringence measurements. We are also grateful for the technical assistance of D. Garreau and J. M. Siffre.

[1] I. Broser and H. Maier, J. Phys. Soc. Japan Suppl. 21, 254 (1966).

[2] A. Suzuki and S. Shionoya, J. Phys. Soc. Japan 31, 1719 (1971).

[3]J. T. Vallin, G. A. Slack, S. Roberts, and A. E. Hughes, Phys. Rev. B 2, 4313 (1970).
[4]G. A. Slack, F. S. Ham, and R. M. Chrenko, Phys. Rev. 152, 376 (1966).
[5]P. Kovacs and E. Lendvay (unpublished).
[6]B. Clerjaud and B. Lambert, J. Phys. E 4, 619 (1971).
[7]D. Smith and J. H. M. Thornley, Proc. Phys. Soc. (London) 89, 779 (1966).
[8]J. L. Prather, Natl. Bur. Std. Monograph No. 19 (U. S. GPO, Washington, D. C., 1961).
[9]A. Räuber and J. Schneider, Z. Naturforsch. 17a, 266 (1962).
[10]R. S. Title, Phys. Rev. 131, 623 (1963).
[11]R. Parrot and G. Tronche, Phys. Status Solidi 41, 217 (1970).
[12]W. M. Walsh, Jr., Phys. Rev. 122, 762 (1961).
[13]W. M. Walsh, Jr. and L. W. Rupp, Jr., Phys. Rev. 126, 952 (1962).
[14]J. Schneider, S. R. Sircar, and A. Räuber, Z. Naturforsch. 18a, 980 (1963).
[15]B. Lambert, T. Buch, and B. Clerjaud, Solid State Commun. 10, 25 (1972).
[16]J. Dieleman, R. S. Title, and W. V. Smith, Phys. Letters 1, 334 (1962).
[17]B. Lambert, T. Buch, and P. Jaszczyn-Kopec, Compt. Rend. 271B, 1232 (1970).
[18]W. M. Walsh, Jr., Phys. Rev. 114, 1473 (1959).
[19]G. Pfister, W. Dreybrodt, and W. Assmus, Phys. Status Solidi 36, 351 (1969).
[20]I. T. Steinberger (private communication).
[21]O. Brafman and I. T. Steinberger, Phys. Rev. 143, 501 (1966).
[22]H. Nelkowski and O. Pfützenreuter, Acta Cryst. A 27, 296 (1971).
[23]C. Barthou, Compt. Rend. 271B, 966 (1970).
[24]D. Curie and C. Barthou, Compt. Rend. 272B, 473 (1971).
[25]R. R. Sharma, T. P. Das, and R. Orbach, Phys. Rev. 149, 257 (1966).
[26]R. R. Sharma, Phys. Rev. B 3, 76 (1971).
[27]G. H. Azarbayejani, Ph. D. thesis (The University of Michigan, 1966) (unpublished).
[28]H. Watanabe and H. Kishishita, Progr. Theoret. Phys. (Kyoto) Suppl. 46, 1 (1970).
[29]T. Buch and A. Gelineau, Phys. Rev. B 4, 1444 (1971).

PHYSICAL REVIEW B VOLUME 7, NUMBER 1 1 JANUARY 1973

# Conversion of Electromagnetic into Acoustic Energy via Indium Films*

A. Zemel and Y. Goldstein
*The Racah Institute of Physics, The Hebrew University, Jerusalem, Israel*
(Received 3 August 1972)

Transverse acoustic waves were generated electromagnetically at 9 GHz using thin indium films on silicon substrates. We report measurements of the conversion efficiency $\alpha$ of electromagnetic into acoustic energy as a function of temperature, magnetic field, and microwave power. The highest conversion efficiency found above the superconducting transition temperature $T_c$ of indium was $5\times10^{-5}$ comparable to that of quartz transducers. Below $T_c$ the conversion efficiency decreases rapidly and becomes magnetic field and microwave power dependent. At low powers a good agreement was found between the experiment and the theory of Abeles with respect to both the value and temperature dependence of $\alpha$. This agreement shows that the generation of the acoustic waves is due primarily to diffuse scattering of electrons at the surfaces of the film. To fit the theory to the experiment we had to assume that diffuse surface scattering persists below $T_c$ as well and thus we conclude that pair scattering at the surface does not conserve momentum. In addition, our results show that $\alpha$ is still appreciable at temperatures well below $T_c$ and thus transverse-phonon generation may possibly be one of the important loss mechanisms in superconducting cavities.

## I. INTRODUCTION

An electromagnetic field in the GHz region incident on a metal film can generate a transverse acoustic wave. The ions and electrons in the metal are accelerated by the electromagnetic field within the penetration depth. For a clean thin film at low temperatures, scattering in the bulk can be neglected, and thus the interaction of the electromagnetic field with the lattice ions may result in the generation of an acoustic wave. There may be another, electronic, contribution to the generation of an acoustic wave. Assuming diffuse surface scattering, the momentum gained from the electromagnetic field by the electrons is transferred to the lattice at the surfaces. This momentum per unit time is a shear force acting on the surface and can also give rise to a transverse acoustic wave.

Experimentally, electromagnetic generation of acoustic waves using indium films was first observed by Abeles[1] and later by the present authors.[2] Theoretically, the problem of electromagnetic generation of transverse acoustic waves in a metal has received considerable attention over the last few years. To calculate the conversion ef-